Composite Structures 226 (2019) 111184

Contents lists available at ScienceDirect

Composite Structures

journal homepage: www.elsevier.com/locate/compstruct

Stress constraint topology optimization using layerwise theory for composite laminates

Jong Wook Lee[a], Jong Jin Kim[a], Gil Ho Yoon[b,*]

[a] Graduate School of Mechanical Engineering, Hanyang University, Republic of Korea
[b] Mechanical Engineering, Hanyang University, Republic of Korea

ARTICLE INFO

Keywords:
Topology optimization
Composite laminate
Layerwise theory
Stress constraint
p-Norm approach
Tsai–Hill criteria

ABSTRACT

An improved stress-based topology optimization method for laminated composites is proposed by applying the layerwise theory in this research. The layerwise theory is an analysis technique for laminated composites or fiber-reinforced composites that has been developed to overcome the disadvantages of the classical laminated plate theory (CLPT). Because transverse shear deformation is ignored in the CLPT, it cannot be used for thick plates or multiple-layered composites. Therefore, new methods have been developed for analyzing them, and one of them is the layerwise theory. Using the layerwise theory, it is possible to accurately analyze a thick plate and predict the behavior of multiple layers of composites. In the layerwise theory, because a new displacement field and a modified finite element (FE) model are used, the FE model of the stress-based topology optimization method (STOM) is reconstructed to apply the layerwise theory. To apply the STOM for composite materials, the specific failure criterion developed for anisotropic materials must be selected. Therefore, the Tsai–Hill criterion and Tsai–Wu criterion are adapted to the STOM formula to consider the failure of composite materials. Further, the orientation of each layer in a composite significantly affects the optimization result as well as stiffness. Therefore, in this study, we optimize the density and orientation simultaneously by setting the orientation as a design variable. Finally, several types of *p*-norm approaches are proposed, and one of them can be chosen depending on the location of the maximum value of the constraint.

1. Introduction

Composite laminates are widely used throughout the industry because they exhibit better mechanical performance than their original counterparts. Many studies on composites have been reported and their performances have been verified through experiments or computational simulations. A composite laminate is generally manufactured by stacking thin composite layers (see Fig. 1). Each layer may have different mechanical properties or strengths. In addition, even with the same anisotropic material, different mechanical properties can be realized depending on the rotation angle of each layer. Initially, the classical plate theory was used to predict the mechanical behaviors of composite laminates [1–3] (See Fig. 2).

The classical plate and shell theories cannot accurately predict the behaviors of thick laminated composite structures because the transverse shear deformation is simplified in these theories [1–3].

It is possible to simplify or ignore shear deformation in thinner composite structures. However, in thicker composite structures, the simplification or disregard of shear deformation causes large errors in predicting the mechanical behavior. To resolve this issue, a shear correction factor is used in the first-order shear deformation theory and a tangential transverse shear effect is used in the high-order theory [3]. Although these methods are applicable in mechanical problems of a single layer, other issues must be solved for applying them to composite laminates composed of several layers. The conventional methods used to analyze a plate or shell cannot implement the zigzag shape of the in-plane displacement of the composite laminate and satisfy the inter-laminar continuity of the transverse stresses of the composite laminate. Many suggestions have been proposed to overcome these issues, and the layerwise theory was introduced to solve the zigzag displacement issue and the interlaminar continuity of the transverse stress issue [3–9]. Unfortunately, this theory is still disadvantageous in that many dominant variables exist depending on the number of layers. Recently, the improved layerwise theory with a smaller number of unknown variables was presented to accurately estimate the stresses or strains and reduce the computational cost [3,5–7].

To design a composite laminate, topology optimization (TO) is used in this research. TO was introduced in the late 1980 s, and many

* Corresponding author at: School of Mechanical Engineering, Hanyang University, Seoul, Republic of Korea.
E-mail address: ghy@hanyang.ac.kr (G.H. Yoon).

https://doi.org/10.1016/j.compstruct.2019.111184
Received 3 October 2018; Received in revised form 3 June 2019; Accepted 26 June 2019
Available online 29 June 2019

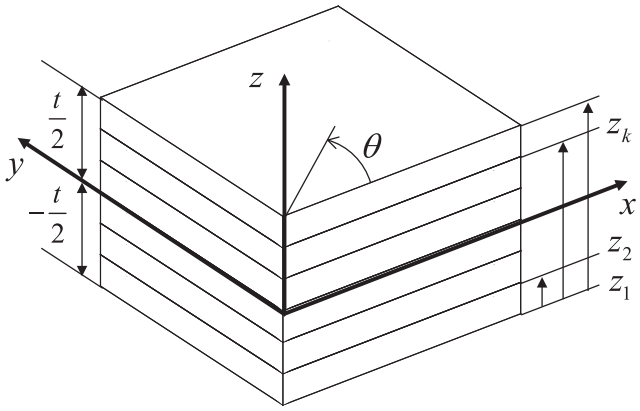

Fig. 1. General configuration of laminate composite structure.

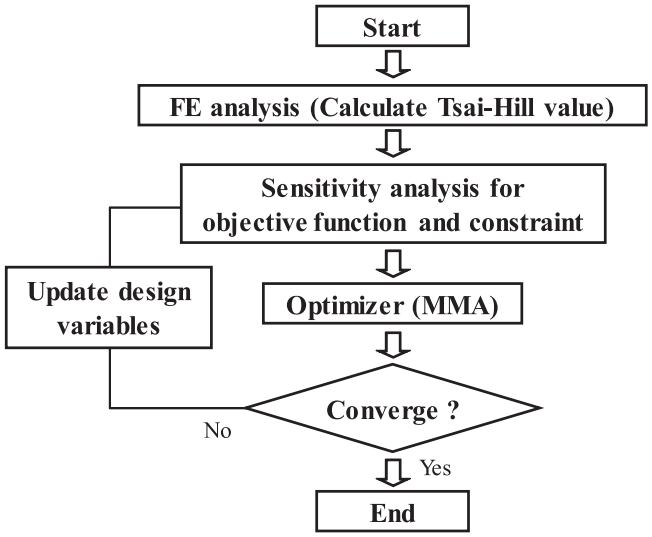

Fig. 2. Flowchart for developed topology optimization method.

investigations and applications have been reported [10–20]. Static failure is a challenging subject in TO applications, and it is generally known as the stress-based topology optimization method (STOM) [21–31]. The STOM cannot easily set the stresses as a constraint owing to the singularity issue or local constraint issue [21,23,25–27,29,32–37]. Recently, the *qp*-relaxation method and the *p*-norm approach have been proposed to solve these issues and the STOM has been widely applied in many fields [21,23,26,27,29,32,33,37]. This study is also one of such applications considering stresses of composite laminates in TO. Some relevant studies about TO for composite laminate have been progressed for a long time [10,19,38–43]. In [38], the material-orthotropy orientation angles and the nodal volume fractions are topologically optimized by the MLPG (Meshless Local Petrov-Galerkin) mixed collocation method. The discrete optimized orientation design of the composite laminate was proposed in [19,40,43]. There has been increasing interest in harvesting energy and studies have been carried out for the application of TO for energy harvesting devices to maximize power generation or electromechanical coupling coefficient. In [38], the piezoelectric energy harvesting system of multilayer plates and shells are topologically optimized [10]. The piezoelectric energy harvesting system maximizing the energy conversion factor was proposed in [39]. The arbitrary fiber orientation for the laminated piezocomposite shell transducer is proposed in [41]. The stress constraints are also included in the design of the laminated piezocomposite energy harvesting devices in [42]. To our best knowledge, most of the related researches have used the classical plate or shell theory to analyze composite laminate. The present study intends to develop a new TO scheme with composite laminate analyzed by the layerwise theory [44,45]. The first issue to be addressed in developing a new TO considering the static failure of composite laminates is that other failure criteria for anisotropic materials are necessary [1,2]. Because a composite material is anisotropic, criteria such as the maximum shear–stress criteria, the distortion energy criteria, and the Coulomb–Mohr criteria developed for isometric materials cannot be used to predict the failures of composite materials [27,46]. As an alternative, the Tsai–Hill criterion that is an extension of the distortional energy yield criterion of von Mises is used in this study [1,2]. Another problem of developing a new TO is the local constraint issue [26,27,29,37]. Because stress is an element-wise property, the number of stresses increases as the number of elements increases. Therefore, as the number of elements increases, the number of constraints also increases. The *p*-norm approach is used to solve this problem because if the *p* value becomes infinitely large, the *p*-norm becomes the maximum value [18,26,27,29,37]. A new issue is that stresses of all layers must be considered in the STOM for composite laminates. Therefore, if the number of layers increases, the problem of the number of constraints increasing also arises. To solve this problem, a modified *p*-norm approach is proposed in this study. The differences between the results obtained through the newly proposed modified *p*-norm approach and that obtained through the existing *p*-norm approach are compared through some numerical examples. Finally, to investigate the influence of each layer orientation in the STOM for composite laminates, the STOM was reformulated by including the orientations of all layers as design variables. Further, the results can be confirmed through numerical examples.

The present paper is organized as follows: in Section 2, the layerwise theory is described briefly. Further, a new STOM is formulated and a sensitivity analysis adapting the layerwise theory is discussed in Section 3. In Section 4, some numerical examples are shown to validate the developed STOM for composite laminates. In Section 5, the conclusions and contributions are presented.

2. Composite laminate structure formulation

2.1. Mathematical theory – Improved layerwise theory

Composite laminate structures consist of thin or thick layers. Three-dimensional FE analysis requires numerous computational resources for an accurate response computation of displacement and stress. To overcome these limitations, some classical plate theories were developed by simplifying or neglecting the influence of transverse shear deformation. As discussed in the introduction, the layerwise theory was developed for overcoming the limitations of classical plate theories [3,5–9,47]. The improved predictions of the displacement and stress are possible using the layerwise theory. The displacement fields in the layerwise theory are approximated as follows [5–7]:

$$\begin{aligned} U_x^k(x,y,z) &= u_x(x,y) + \phi_x(x,y)z + \theta_x^k(x,y)g(z) + \psi_x^k(x,y)h(z) \\ U_y^k(x,y,z) &= u_y(x,y) + \phi_y(x,y)z + \theta_y^k(x,y)g(z) + \psi_y^k(x,y)h(z) \\ U_z^k(x,y,z) &= w(x,y) \end{aligned} \tag{1}$$

where U_x^k and U_y^k denote the in-plane displacements of the k-th layer of the laminate, and U_z^k denotes the transverse deflection of the k-th layer or the ply of the laminate. The quantities u_x, u_y, and w denote the displacements of the reference plane. The rotations of the normal to the reference plane about the x and y axes are ϕ_x and ϕ_y, respectively. The terms θ_x^k, θ_y^k, ψ_x^k, and ψ_y^k are the layerwise structural unknowns defined at the k-th ply. The through-laminate-thickness functions, $g(z)$ and $h(z)$, are used to address the characteristics of the in-plane zigzag deformations, which are of the following forms:

$$g(z) = \sinh(z/t)$$
$$h(z) = \cosh(z/t) \tag{2}$$

where t is the total thickness of the laminate structure, and the functions $g(z)$ and $h(z)$ render high-order odd and even distributions, respectively.

The assumed layerwise displacement field can be further simplified by applying the structural constraints [5–7] to reduce the number of structural variables. In this study, the applied structural conditions are the traction free boundary conditions on the top and bottom, and continuity conditions of transverse shear stress and in-plane displacement on each interlaminar. By applying these conditions, the modified in-plane displacement fields are presented as follows:

$$U_x^k(x,y,z) = u_x + A_x^k(z)\phi_x + B_x^k(z)\phi_y + C_x^k(z)w_{,x} + D_x^k(z)w_{,y}$$
$$U_y^k(x,y,z) = u_y + A_y^k(z)\phi_x + B_y^k(z)\phi_y + C_y^k(z)w_{,x} + D_y^k(z)w_{,y} \tag{3}$$

where

$$\begin{aligned} A_x^k(z) &= z + a_x^k g(z) + c_x^k h(z) & A_y^k(z) &= a_y^k g(z) + c_y^k h(z) \\ B_x^k(z) &= b_x^k g(z) + d_x^k h(z) & \cdots \quad B_y^k(z) &= z + b_y^k g(z) + d_y^k h(z) \\ C_x^k(z) &= a_x^k g(z) + c_x^k h(z) & C_y^k(z) &= a_y^k g(z) + c_y^k h(z) \\ D_x^k(z) &= b_x^k g(z) + d_x^k h(z) & D_y^k(z) &= b_y^k g(z) + d_y^k h(z) \end{aligned} \tag{4}$$

Because the in-plane displacement fields consist of u_x, u_y, w, ϕ_x, ϕ_y, $w_{,x}$, and $w_{,y}$, it is independent from the number of layers. The layerwise coefficients, a_x^k, a_y^k, b_x^k, b_y^k, c_x^k, c_y^k, d_x^k, and d_y^k, are obtained from the constraint equations (the more details are presented in [5,6]), and are expressed in terms of the laminate geometry and material properties [5,6].

2.2. Finite element implementation

Certain procedures should be introduced to implement the layerwise theory into the finite element model. The linear Lagrange interpolation function is employed to interpolate the in-plane displacements, whereas the Hermite cubic interpolation function is used for the out-of-plane displacement interpolation [5,6].

$$(u_x,\ u_y,\ \phi_x,\ \phi_y) = \sum_{m=1}^{n} N_m(x,y)[(u_x)_m,\ (u_y)_m,\ (\phi_x)_m,\ (\phi_y)_m] \tag{5}$$

$$w = \sum_{m=1}^{n} [H_m(z)(w)_m + H_{xm}(z)(w_{,x})_m + H_{ym}(z)(w_{,y})_m] \tag{6}$$

where N_m represents the Lagrange interpolation function, and H_m, H_{xm}, and H_{ym} represent the Hermite interpolation functions. The number of nodes in each element is n. The displacements in the x- and y-direction, and the rotations of the normal to the reference plane about the x and y axes at the m-th node in each element are denoted by $(u_x)_m$, $(u_y)_m$, $(\phi_x)_m$, and $(\phi_y)_m$, respectively. The displacement in the z-direction and the partial derivatives for the x and y directions at the m-th node in each element are w_m, $(w_{,x})_m$, and $(w_{,y})_m$, respectively.

$$\mathbf{KU} = \mathbf{F} \tag{7}$$

$$\mathbf{u}_e = \mathbf{NU} \tag{8}$$

$$\mathbf{u}_e = [u_x,\ u_y,\ w,\ \phi_x,\ \phi_y]^{\mathrm{T}} \tag{9}$$

$$\mathbf{N} = \begin{bmatrix} N_m & 0 & 0 & 0 & 0 & 0 & 0 \\ 0 & N_m & 0 & 0 & 0 & 0 & 0 \\ \cdots\ 0 & 0 & H_m & H_{xm} & H_{ym} & 0 & 0\ \cdots \\ 0 & 0 & 0 & 0 & 0 & N_m & 0 \\ 0 & 0 & 0 & 0 & 0 & 0 & N_m \end{bmatrix} \tag{10}$$

where $\mathbf{K}$ and $\mathbf{F}$ are denoting the global stiffness matrix and the global force vector, respectively. The global displacement, the displacement of the e-th element, and the shape function are $\boldsymbol{U}$, $\mathbf{u}_e$, and $\mathbf{N}$, respectively.

$$\mathbf{KU} = \mathbf{F} \tag{11}$$

$$\mathbf{k}_e = \iiint_{V_e} \mathbf{B}^{\mathrm{T}}\mathbf{Q}_e\mathbf{B}dV \tag{12}$$

$$\mathbf{B} = \mathbf{LN} \tag{13}$$

$$\mathbf{L} = \begin{bmatrix} \frac{\partial}{\partial x} & 0 & C_1^k\frac{\partial^2}{\partial x^2} + D_1^k\frac{\partial^2}{\partial x\partial y} & A_1^k\frac{\partial}{\partial x} & B_1^k\frac{\partial}{\partial x} \\ 0 & \frac{\partial}{\partial y} & C_2^k\frac{\partial^2}{\partial x\partial y} + D_2^k\frac{\partial^2}{\partial y^2} & A_2^k\frac{\partial}{\partial y} & B_2^k\frac{\partial}{\partial y} \\ 0 & 0 & 0 & 0 & 0 \\ 0 & 0 & C_{2,z}^k\frac{\partial}{\partial x} + (1 + D_{2,z}^k)\frac{\partial}{\partial y} & A_{2,z}^k & B_{2,z}^k \\ 0 & 0 & (C_{1,z}^k + 1)\frac{\partial}{\partial x} + D_{1,z}^k\frac{\partial}{\partial y} & A_{1,z}^k & B_{1,z}^k \\ \frac{\partial}{\partial y} & \frac{\partial}{\partial x} & C_2^k\frac{\partial^2}{\partial x^2} + (C_1^k + D_2^k)\frac{\partial^2}{\partial x\partial y} & A_1^k\frac{\partial}{\partial y} + A_2^k\frac{\partial}{\partial x} & B_1^k\frac{\partial}{\partial y} + B_2^k\frac{\partial}{\partial x} \\ & & + D_1^k\frac{\partial^2}{\partial y^2} & & \end{bmatrix} \tag{14}$$

where the global stiffness, global force, e-th elementary stiffness matrix, and constitutive matrix are denoted by $\mathbf{K}$ and $\mathbf{F}$, $\mathbf{k}_e$, and $\mathbf{Q}_e$, respectively. To reflect the influence due to the angle, the constitutive matrix is defined as follows:

$$\mathbf{Q}_e = \gamma_e^{n_k}\bar{\mathbf{Q}}_0 \tag{15}$$

The design variable and the penalty value are denoted by γ_e and n_k, respectively. To consider a rotational angle (θ) of the ply, the transformation matrices, $\mathbf{T}_1$ and $\mathbf{T}_2$, are multiplied.

$$\bar{\mathbf{Q}}_0 = \mathbf{T}_1^{-1}\mathbf{Q}_0\mathbf{T}_2 \tag{16}$$

$$\mathbf{T}_1 = \begin{bmatrix} \cos^2\theta & \sin^2\theta & 0 & 0 & 0 & 2\cos\theta\sin\theta \\ \sin^2\theta & \cos^2\theta & 0 & 0 & 0 & -2\cos\theta\sin\theta \\ 0 & 0 & 1 & 0 & 0 & 0 \\ 0 & 0 & 0 & \cos\theta & -\sin\theta & 0 \\ 0 & 0 & 0 & \sin\theta & \cos\theta & 0 \\ -\cos\theta\sin\theta & \cos\theta\sin\theta & 0 & 0 & 0 & \cos^2\theta - \sin^2\theta \end{bmatrix} \tag{17}$$

$$\mathbf{T}_2 = \begin{bmatrix} \cos^2\theta & \sin^2\theta & 0 & 0 & 0 & \cos\theta\sin\theta \\ \sin^2\theta & \cos^2\theta & 0 & 0 & 0 & -\cos\theta\sin\theta \\ 0 & 0 & 1 & 0 & 0 & 0 \\ 0 & 0 & 0 & \cos\theta & -\sin\theta & 0 \\ 0 & 0 & 0 & \sin\theta & \cos\theta & 0 \\ -2\cos\theta\sin\theta & 2\cos\theta\sin\theta & 0 & 0 & 0 & \cos^2\theta - \sin^2\theta \end{bmatrix} \tag{18}$$

The term $\mathbf{Q}_o$ represents the three-dimensional constitutive matrix for an orthotropic material.

$$\mathbf{Q}_0 = \Gamma \cdot \begin{bmatrix} E_1(1-\nu_{23}\nu_{32}) & E_1(\nu_{21}+\nu_{31}\nu_{23}) & E_1(\nu_{31}+\nu_{21}\nu_{32}) & 0 & 0 & 0 \\ E_1(\nu_{21}+\nu_{31}\nu_{23}) & E_2(1-\nu_{13}\nu_{31}) & E_2(\nu_{32}+\nu_{12}\nu_{31}) & 0 & 0 & 0 \\ E_1(\nu_{31}+\nu_{21}\nu_{32}) & E_2(\nu_{32}+\nu_{12}\nu_{31}) & E_3(1-\nu_{12}\nu_{21}) & 0 & 0 & 0 \\ 0 & 0 & 0 & G_{23} & 0 & 0 \\ 0 & 0 & 0 & 0 & G_{13} & 0 \\ 0 & 0 & 0 & 0 & 0 & G_{12} \end{bmatrix} \tag{19}$$

$$\Gamma = \frac{1}{1 - \nu_{12}\nu_{21} - \nu_{23}\nu_{32} - \nu_{31}\nu_{13} - 2\nu_{21}\nu_{32}\nu_{13}} \tag{20}$$

where E_i, G_{ij}, and represent the Young's modulus in the i-direction, the shear modulus in the ij-plane, and Poisson's ratio between the i and j directions. Further, the stresses at the center of each element are evaluated by Eq. (21).

$$\boldsymbol{\sigma}_e^k = \gamma^{n_s}\bar{\mathbf{Q}}_0\boldsymbol{\varepsilon}_e^k \tag{21}$$

The stress and strain of the e-th element of the k-th layer is denoted by $\boldsymbol{\sigma}_e^k$ and $\boldsymbol{\varepsilon}_e^k$, respectively. The penalty factor, n_s, was set to 0.5 to avoid the singularity issue mentioned by many researchers. In finite element model, the layerwise theory is employed [3,5–7]. This approach has an advantage in terms of computation accuracy and efficiency. All layers share the same nodes for each element.

3. Topology optimization formulation and sensitivity analysis

3.1. Topology optimization formulation

In this section, a new stress-based TO method for composite laminate using the layerwise theory is formulated. The objective function is set to minimize the volume, and the constraint is set such that the stress state within the design domain satisfies the Tsai–Hill criterion. The Tsai–Hill criterion is used in this study because the composite laminate is an anisotropic material [1,2]. In most related studies on STOM developed for isotropic materials, a von Mises yield criterion was generally used to determine structural failure. (Nevertheless, there are various criteria according to the characteristics of the material, and the appropriate methods are used according to the situation.) [27,29]. The composite laminate is an anisotropic material for which an appropriate criterion must be used; the Tsai–Hill criterion is used in this study.

$$\begin{aligned} &\underset{\gamma,\theta}{\text{Minimize}}\ V(\tilde{\boldsymbol{\gamma}}) = \textstyle\sum_{e=1}^{NE} \tilde{\gamma}_e v_e \ (\tilde{\boldsymbol{\gamma}}\text{:filtered density}) \\ &\text{Subject to } g_{\max}(\tilde{\boldsymbol{\gamma}}, \theta) \leqslant 1 \\ &g_{\max}(\tilde{\boldsymbol{\gamma}}, \theta) = \max(g_e^k(\tilde{\boldsymbol{\gamma}}, \theta)),\ \ e = 1, ...,NE,\ \ k = 1, ...,NL \\ &\tilde{\boldsymbol{\gamma}} = \Xi(\boldsymbol{\gamma}) \text{ with the density filter } \Xi \end{aligned} \tag{22}$$

where the total volume, the e-th element volume, the Tsai–Hill value of the k-th layer of the e-th element, and the design variable are denoted by V, v_e, g_e^k, and $\boldsymbol{\gamma}$, respectively. Additionally, the NE and NL represent the numbers of element and layer. In this study, the Tsai–Hill value is used in the Tsai–Hill criterion to determine whether the structure is broken [1,2].

$$\begin{aligned} g_e^k &= F(\sigma_2^k - \sigma_3^k)^2 + G(\sigma_3^k - \sigma_1^k)^2 + H(\sigma_1^k - \sigma_2^k)^2 + 2L(\tau_{23}^k)^2 + 2M \\ &\quad (\tau_{31}^k)^2 + 2N(\tau_{12}^k)^2 \end{aligned} \tag{23}$$

$$F = \frac{1}{2}\left(\frac{1}{Y^2} + \frac{1}{Z^2} - \frac{1}{X^2}\right),\ \ G = \frac{1}{2}\left(\frac{1}{X^2} + \frac{1}{Z^2} - \frac{1}{Y^2}\right),\ \ H = \frac{1}{2}\left(\frac{1}{X^2} + \frac{1}{Y^2} - \frac{1}{Z^2}\right)$$
$$L = \frac{1}{2Q^2},\ \ M = \frac{1}{2R^2},\ \ N = \frac{1}{2S^2} \tag{24}$$

where σ_1^k, σ_2^k, σ_3^k, τ_{23}^k, τ_{31}^k, and τ_{12}^k represent the stresses expressed in the principal material coordinates (or ply coordinates). The notation X represents the ultimate normal stress magnitudes in the fiber direction, whereas Y and Z indicate the ultimate normal stress magnitudes in the two transverse directions. The notation S indicates the ultimate shear stress in the plane of the lamina, whereas Q and R indicate the ultimate interlaminar shear stresses in the plane perpendicular to the lamina plane [1,2]. Note that one of the reasons to employ the Tasi-Hill value is to predict the failure of anisotropic material. The Tasi-Hill value also can be regarded as one of the extensions of the von-Mises stress for anisotropic material. In addition to the Tsai–Hill criterion, the following Tsai–Wu criterion formulated in Eq. (25) can be setup for topology optimization in order to consider the fractures of the composite material.

$$\begin{aligned} g_e^k &= \frac{(\sigma_1^k)^2}{X_t X_c} + \frac{(\sigma_2^k)^2}{Y_t Y_c} + \frac{(\sigma_3^k)^2}{Z_t Z_c} + \frac{(\sigma_4^k)^2}{S^2} + \frac{(\sigma_5^k)^2}{R^2} + \frac{(\sigma_6^k)^2}{Q^2} \\ &+ \left(\frac{1}{X_t} - \frac{1}{X_c}\right)\sigma_1^k + \left(\frac{1}{Y_t} - \frac{1}{Y_c}\right)\sigma_2^k + \left(\frac{1}{Z_t} - \frac{1}{Z_c}\right)\sigma_3^k + F_{12}\sigma_1^k\sigma_2^k + F_{13}\sigma_1^k\sigma_3^k \\ &+ F_{23}\sigma_2^k\sigma_3^k \end{aligned} \tag{25}$$

where the notation X_t and X_t represent the ultimate normal tensile and the compression stress magnitudes in the fiber direction, respectively. The ultimate normal tensile and the compression stress magnitudes in the two transverse directions are denoted by Y_t, Y_c, Z_t, and Z_c, respectively. The Tsai–Wu criterion is advantageous as it can consider more accurate fracture than the Tsai–Hill criterion. The coefficients F_{12}, F_{13}, and F_{23} of the last three terms of Eq. (25) can be determined with some experiments. Often the last three terms of Eq. (25) can be simply modified as follows:

$$F_{12} = \frac{1}{\sqrt{X_t X_c Y_t Y_c}},\ \ F_{23} = \frac{1}{\sqrt{Y_t Y_c Z_t Z_c}},\ \ F_{13} = \frac{1}{\sqrt{X_t X_c Z_t Z_c}} \tag{26}$$

We use the p-norm approach in this study to obtain the maximum Tsai-Hill value in the design domain shown in Eq. (22). However, a problem arises because the number of stresses to be included is equal to the product of the total number of layers and the number of elements. In the previous research on the stress-based TO method, only a single layer existed because only the stresses of the total number of elements were considered. However, more stresses should be considered in this study. Nevertheless, there are situations where stresses in all layers are not taken considered. For example, it is not necessary to consider the stress of the entire layer if the distributions of the stresses in all the layers are constant, or if the stress values of a specific layer are significantly larger than the stress values of the other layers. In these cases, the maximum stress value can be found by considering the stress values of one specific layer. With in-plane load, the stresses become constant along the thickness direction and only the consideration of the stress value of one layer is enough in optimization. With a layered structure especially with out-of-plane load, the stress values of all layers are naturally different, and they should be considered to find out the maximum stress value. Therefore, in this study, we present two types of p-norm approaches—a p-norm approach considering the stresses of all layers and another p-norm approach considering the stresses of a certain layer. The two modified types of p-norm approaches can be rewritten as follows.

Type 1) The location of the maximum Tsai–Hill value is unknown:

$$g_{\max} \equiv\ C_T^{iter}\langle g_T^{PN}\rangle = C_T^{iter}\left[\sum_{k=1}^{NL}\left\{\sum_{e=1}^{NE}(g_e^k)^p\tilde{\gamma}_e\right\}\right]^{\frac{1}{p}} \tag{27}$$

$$C_T^{iter} = \alpha\frac{g_{\max}^{iter-1}}{\langle g_T^{PN}\rangle^{iter-1}} + (1-\alpha)C_T^{iter-1} 0 < \alpha < 1 \tag{28}$$

Type 2) The location of the maximum Tsai–Hill value is known:

$$g_{\max} \equiv\ C_S^{iter}\langle g_S^{PN}\rangle = C_S^{iter}\left(\sum_{e=1}^{NE}(g_e^{obj})^p\tilde{\gamma}_e\right)^{\frac{1}{p}} \tag{29}$$

$$C_S^{iter} = \alpha\frac{g_{\max}^{iter-1}}{\langle g_S^{PN}\rangle^{iter-1}} + (1-\alpha)C_S^{iter-1}\cdot 0 < \alpha < 1 \tag{30}$$

where the correction factor at the $iter$-th optimization iteration is denoted as C_T^{iter} or C_S^{iter} depending on whether the stresses of all layers or those of certain layers are selected. The correction factor (C) in Eqs. (28) and (30) were proposed in order to adjust the p-norm value of Tsai-Hill value closed to the maximum Tsai-Hill value. The coefficient p used in the p-norm approach must be infinite, but a relatively large is used due to the numerical stability. Some differences exist between the real maximum value and the p-norm value. To remedy these differences, the correction factor was proposed in the stress-based topology optimization (see [27,29]) and the same procedure can be used for the present study. In this study, 3 is used for the coefficient p. The correction factor serves to help the p-norm of the Tsai-Hill value closer to the maximum Tsai-Hill value. Inevitably, some differences exist between the p-norm value and the actual maximum value. To reduce this gap, the correction factor was proposed (see [27,29]). For an example 1, the p-norm value

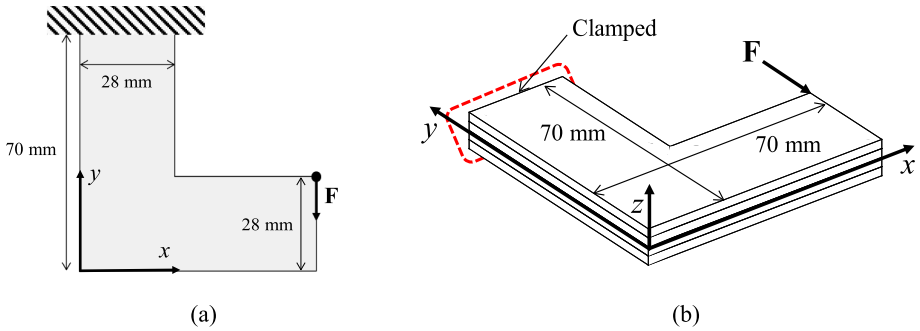

Fig. 3. Configuration of design domain and boundary conditions: (a) two-dimensional geometry of design domain and (b) three-dimensional geometry of the design domain (the number of layers is four, and the total thickness is 1 mm).

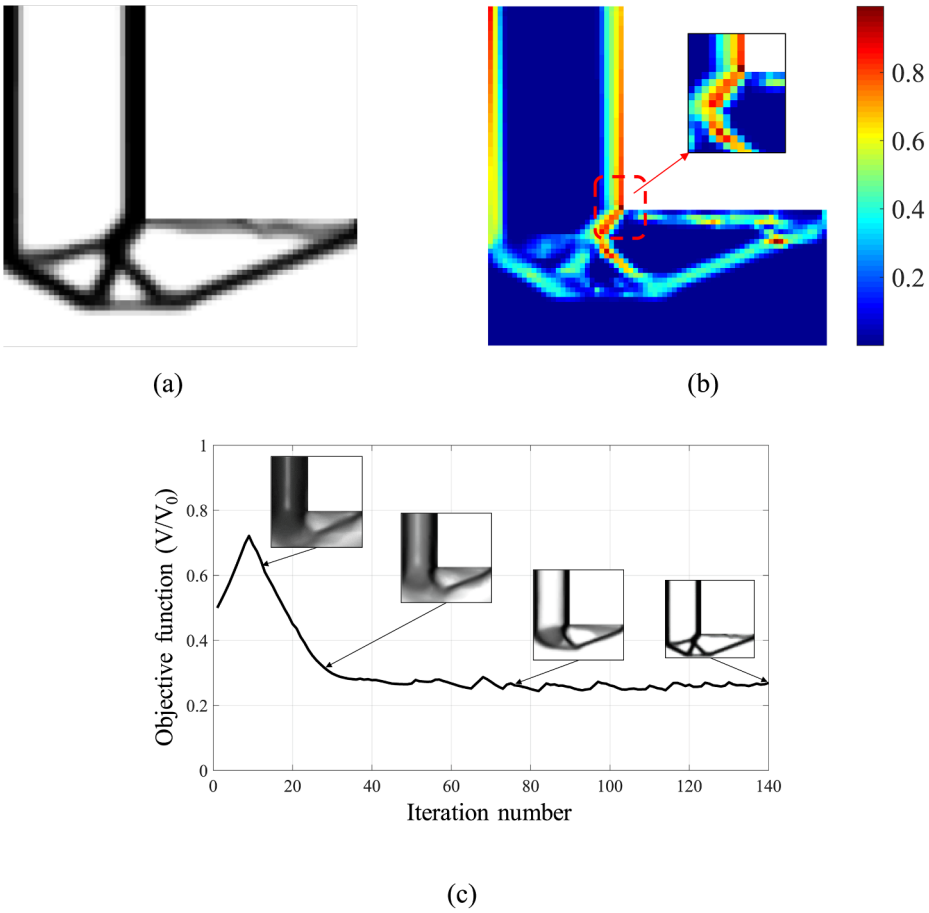

Fig. 4. Optimization result and the Tsai-Hill distribution (the converged volume: 26.92% and the maximum Tsai–Hill value: 0.9932): (a) an optimized layout, (b) the distribution of Tsai–Hill value and (c) the history of the objective function.

of the Tsai-Hill value is 7.1638 whereas the actual maximum Tsai-Hill value is 0.9932 in Fig. 4. Therefore, the correction factor was set to 0.1452. Further, $g_{\max}^{iter}$, g_e^{obj}, p, and α are the actual maximum value of the constraint functions in the design domain, the Tsai-Hill value or Tsai-Wu value of the e-th element in the *obj*-th layer, the coefficient p for the p-norm method, and the damping factor, respectively. The αvalue is set to 0.5 in this study.

3.2. Sensitivity analysis

It is essential to derive the sensitivity of the Tsai–Hill value in order to apply a gradient-based optimizer. For an optimization algorithm, the method of moving asymptotes was used [48]. The following sensitivity analysis can be formulated with the adjoint variable λ. There are two different sensitivity analysis formulations corresponding to the two choices—the total stress of the layers or the stress of a selected layer. If all stresses in the design domain and all layers are considered, the sensitivity analysis can be expressed as follows.

$$\frac{d\langle g_T^{PN}\rangle}{d\widetilde{\gamma}_e} = \frac{\partial\langle g_T^{PN}\rangle}{\partial\widetilde{\gamma}_e} + \sum_{k=1}^{NL}\frac{\partial\langle g_T^{PN}\rangle}{\partial g_e^k}\frac{\partial g_e^k}{\partial\boldsymbol{\sigma}_e^k}\frac{\partial\boldsymbol{\sigma}_e^k}{\partial\widetilde{\gamma}_e} + \sum_{k*=1}^{NL}\sum_{e*=1}^{NE}\frac{\partial\langle g_T^{PN}\rangle}{\partial g_{e*}^{k*}}\frac{\partial g_{e*}^{k*}}{\partial\boldsymbol{\sigma}_{e*}^{k*}}\frac{\partial\boldsymbol{\sigma}_{e*}^{k*}}{\partial\mathbf{U}}\frac{d\mathbf{U}}{d\widetilde{\gamma}_e} \tag{31}$$

The adjoint variable $\boldsymbol{\lambda}$ for sensitivity is computed through derivative of static equilibrium as follows.

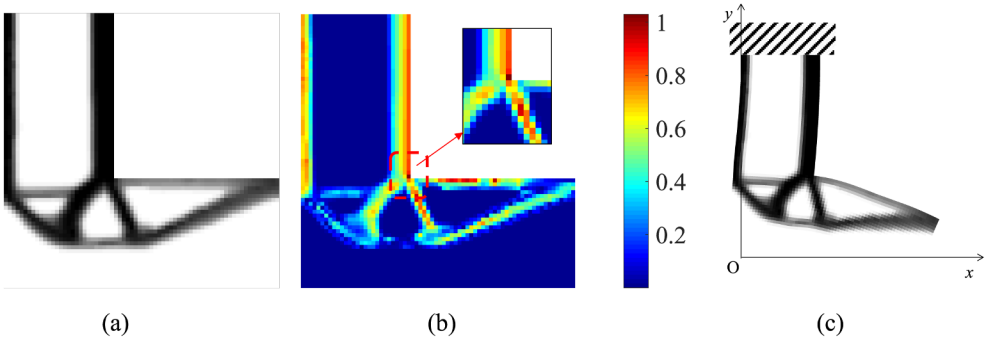

Fig. 5. Optimization result and the Tsai–Wu value distribution (the converged volume: 26.57% and the maximum Tsai–Wu value: 0.9964): (a) an optimized layout, (b) the distribution of the Tsai–Wu value and (c) the deformed shape (Deformation scaling : 5).

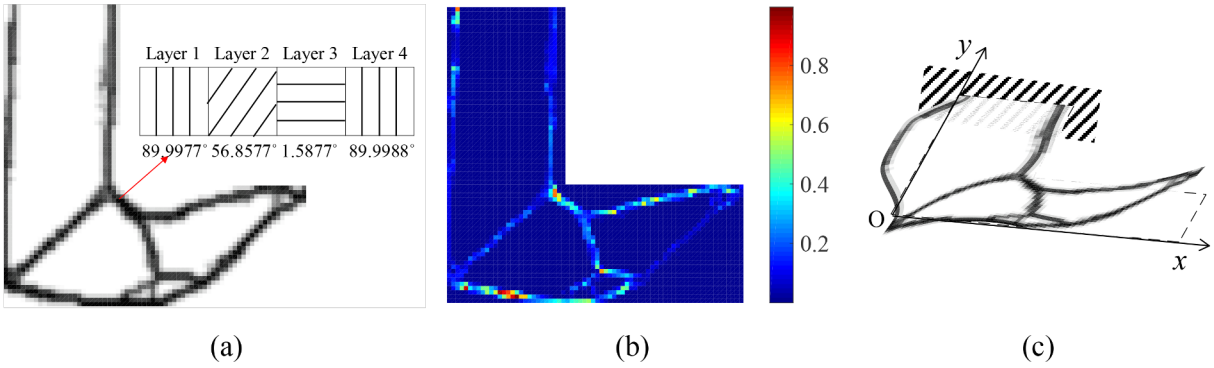

Fig. 6. An optimization result without the symmetric angle condition: (a) an optimized layout, (b) the Tsai–Hill value distribution and (c) 3D deformation plot with the out-of-plane displacement (Deformation scaling: 5).

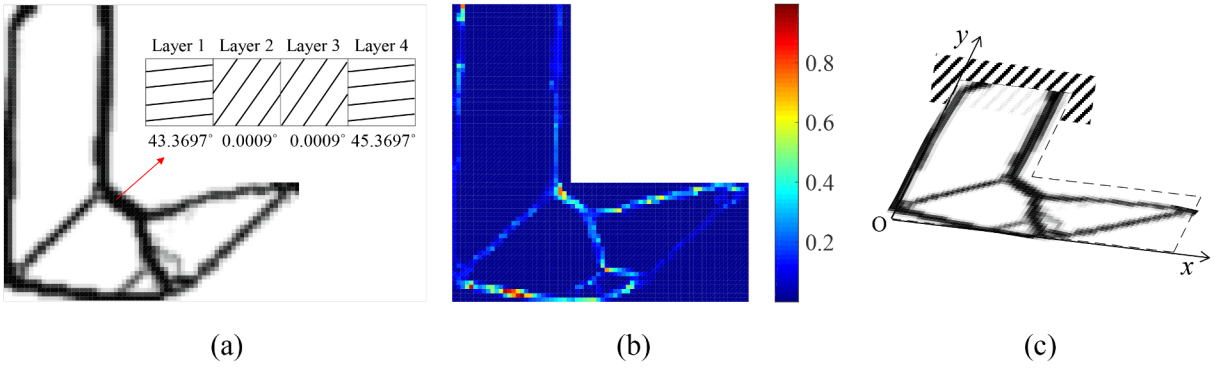

Fig. 7. An optimization result with symmetric angle condition: (a) an optimized layout, (b) the Tsai–Hill value distribution and (c) 3D deformation plot with the out-of-plane displacement (Deformation scaling: 5).

$$\mathbf{K}\frac{d\mathbf{U}}{d\tilde{\gamma}_e} = \frac{d\mathbf{F}}{d\tilde{\gamma}_e} - \frac{d\mathbf{K}}{d\tilde{\gamma}_e}\mathbf{U}, \quad \frac{d\mathbf{U}}{d\tilde{\gamma}_e} = 0 \tag{32}$$

$$\lambda^{\mathrm{T}} = -\sum_{k*=1}^{NL}\sum_{e*=1}^{NE}\frac{\partial\langle g_T^{PN}\rangle}{\partial g_{e*}^{k*}}\frac{\partial g_{e*}^{k*}}{\partial \sigma_{e*}^{k*}}\frac{\partial \sigma_{e*}^{k*}}{\partial \mathbf{U}}\mathbf{K}^{-1} \tag{33}$$

$$\mathbf{K}^{\mathrm{T}}\lambda = -\sum_{k^*=1}^{NL}\sum_{e*=1}^{NE}\frac{\partial\langle g_T^{PN}\rangle}{\partial g_{e*}^{k*}}\left(\frac{\partial g_{e*}^{k*}}{\partial \sigma_{e*}^{k*}}\frac{\partial \sigma_{e*}^{k*}}{\partial \mathbf{U}}\right)^{\mathrm{T}} \tag{34}$$

The final sensitivity values of the p-norm stress can thus be obtained.

$$\frac{d\langle g_T^{PN}\rangle}{d\tilde{\gamma}_e} = \frac{\partial\langle g_T^{PN}\rangle}{\partial\tilde{\gamma}_e} + \sum_{k=1}^{NL}\frac{\partial\langle g_T^{PN}\rangle}{\partial g_e^k}\frac{\partial g_e^k}{\partial \sigma_e^k}\frac{\partial \sigma_e^k}{\partial\tilde{\gamma}_e} + \lambda^{\mathrm{T}}\frac{d\mathbf{K}}{d\tilde{\gamma}_e}\mathbf{U} \tag{35}$$

Similarly, the sensitivity for the angles can be derived as follows.

$$\frac{d\langle g_T^{PN}\rangle}{d\theta_k} = \sum_{e=1}^{NE}\frac{\partial\langle g_S^{PN}\rangle}{\partial g_e^k}\frac{\partial g_e^k}{\partial \sigma_e^k}\frac{\partial \sigma_e^k}{\partial\theta_k} + \hat{\lambda}^{\mathrm{T}}\frac{d\mathbf{K}}{d\theta_k}\mathbf{U} \tag{36}$$

$$\mathbf{K}\frac{d\mathbf{U}}{d\theta_k} = \frac{d\mathbf{F}}{d\theta_k} - \frac{d\mathbf{K}}{d\theta_k}\mathbf{U}, \quad \frac{d\mathbf{F}}{d\theta_k} = 0 \tag{37}$$

$$\hat{\lambda}^{\mathrm{T}} = -\sum_{k*=1}^{NL}\sum_{e*=1}^{NE}\frac{\partial\langle g_S^{PN}\rangle}{\partial g_{e*}^{k*}}\left(\frac{\partial g_{e*}^{k*}}{\partial \sigma_{e*}^{k*}}\frac{\partial \sigma_{e*}^{k*}}{\partial \mathbf{U}}\right)^{\mathrm{T}}\mathbf{K}^{-1} \tag{38}$$

$$\mathbf{K}^{\mathrm{T}}\hat{\lambda} = -\sum_{k*=1}^{NL}\sum_{e*=1}^{NE}\frac{\partial\langle g_S^{PN}\rangle}{\partial g_{e*}^{k*}}\left(\frac{\partial g_{e*}^{k*}}{\partial \sigma_{e*}^{k*}}\frac{\partial \sigma_{e*}^{k*}}{\partial \mathbf{U}}\right)^{\mathrm{T}} \tag{39}$$

The first term of $\frac{d\langle g_T^{PN}\rangle}{d\theta_k}$ is the derivatives of the p-norm defined in Eq. (27) with respect to the k-th angle. The third term in Eq. (31) indicates that all layers and all elements affect the derivative of displacement with respect to the design variable with the p-norm approach

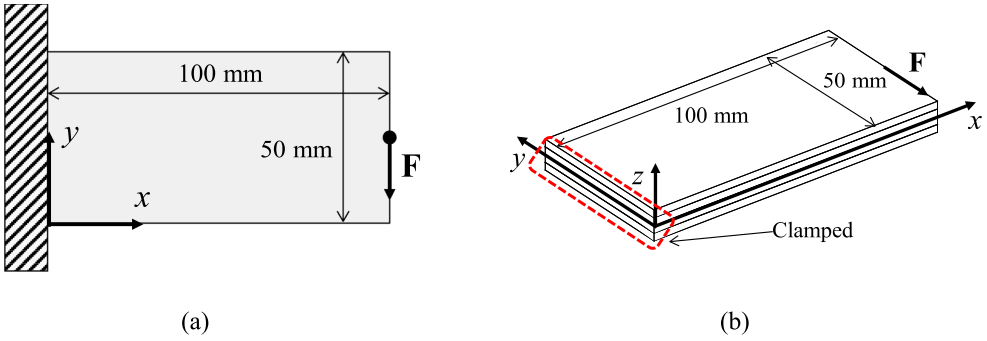

Fig. 8. Configuration of design domain and boundary conditions: (a) two-dimensional geometry of design domain and (b) three-dimensional geometry of the design domain (the number of layers is four, and the total thickness is 1 mm).

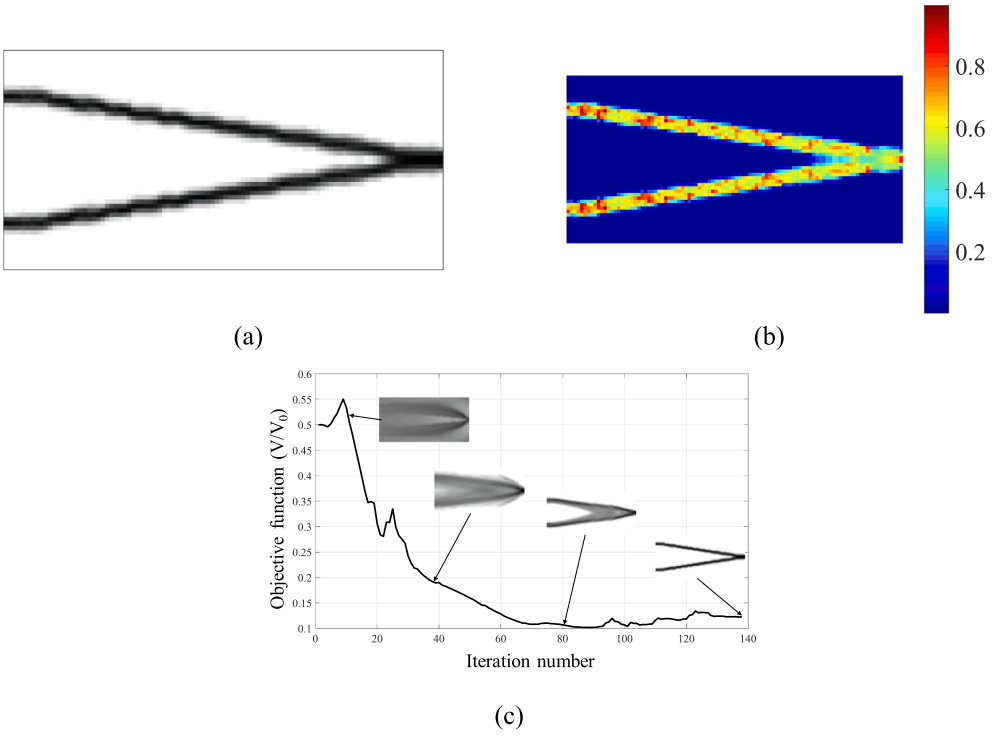

Fig. 9. Optimized shape and the Tsai–Hill value distribution considering all layers (the converged volume: 11.21% and the maximum Tsai–Hill value is 0.9936): (a) an optimized shape and (b) the distribution of Tsai–Hill value and (c) the history of the objective function.

considering the stress values of all layers. The optimization procedure can be found in the flowchart.

4. Numerical examples

Some numerical examples are considered in this section to validate the developed TO method. We use the method of moving asymptotes for the gradient-based optimizer [48].

4.1. Example 1: L-bracket problem

For the first numerical example, Fig. 3 shows an L-shaped bracket structure, which is a benchmark problem for stress-based TO. Relevant research has shown that structures with rounded corners are preferred to prevent stress concentration at the corners [27–29]. We discuss the validity, unique features, and usefulness of our approach by comparing the optimized layouts of the stress-based TO design for the composite laminate and our proposed design.

Fig. 3(a) shows the detailed geometry and boundary conditions. The load applied is 0.05 N and the thickness of the composite laminate is 1 mm. All degree of freedom of displacements are set to zeros along the boundary condition and the load was uniformly applied to all layers. One of the reasons to consider the in-plan loading conditions is to illustrate some differences in terms of the optimized layout using the layerwise theory compared with the optimized layout using the plane-stress problem. The in-plane displacement fields of the layerwise theory is formulated by combining the displacement field of the classical plate theory and the two additional terms as shown in Eq. (1) to improve the accuracy. Furthermore, through this example, it is possible to observe and compare the optimized layouts by the computation of the present layerwise theory and the classical plate theory in case of the in-plane load. The effect of the out-of-plane load will be considered. This example comprises four layers. All layers of composite laminate in all examples have different orientations and all angles can be changed independently. In this example, to get only material distribution, angles of all layer are fixed as 0°. In this example the angle of each layer is

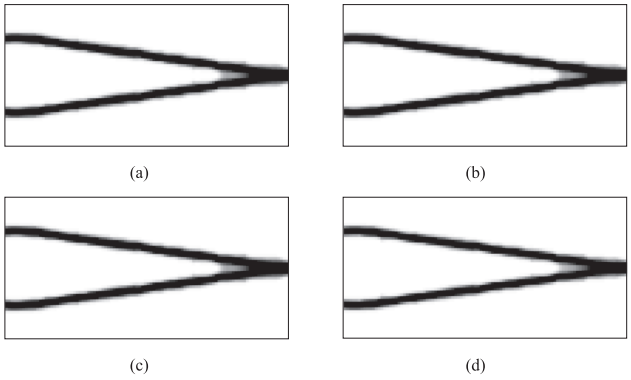

Fig. 10. Optimized shapes with different constraints: (a) considering maximum Tsai–Hill value of 1st layer (converged volume: 11.63%), (b) considering maximum Tsai–Hill value of 2nd layer (converged volume: 11.64%), (c) considering maximum Tsai–Hill value of 3rd layer (converged volume: 11.67%) and (d) considering maximum Tsai–Hill value of 4th layer (converged volume: 11.11%).

fixed at 0° to avoid effect of angle. Composite laminate can be made by several stacked layers to get improved mechanical properties, i.e., stiffness or strength. To consider a stacked composite layer, topology optimization with multiple layers with a specific angle orientation or orientational angles of each layer are considered. The material used in this example is TM800s/M21, and the material properties are as follows: $E_1 = 135$ GPa, $E_2 = E_3 = 7.64$ GPa, $G_{12} = G_{13} = 5.61$ GPa, $G_{23} = 2.75$ GPa, $v_{12} = v_{13} = 0.35$, $v_{23} = 0.4$, and$X = 165$ GPa, $Y = 45$ MPa, $Z = 45$ MPa, $Q = 50$ MPa, $R = 50$ MPa , $S = 50$ MPa. The optimized shape can be obtained from Fig. 4 through the developed optimization algorithm. It is noteworthy that the *p*-norm approach used to obtain the maximum stress value is based on the stress of the entire layer.

Black and white figure in Fig. 4(a) represents 2-dimensional (in *x*-*y* plane) optimized layout of composite laminate and all subsequent optimized layouts are presented in the same way. It is assumed that all layers have the same planar layout to avoid bonding problems at the interfaces among layers due to the shape differences of each layer in all examples. That implies that all layers share the same design variable. As shown in Fig. 4(a), it is impossible to obtain a shape similar to the optimized layout obtained with isotropic materials. The fact that stress concentration can be prevented is shown in Fig. 4(b). From the Tsai–-Hill value distribution, we confirmed that the stress was not concentrated on the corner portion but dispersed to the periphery. Some gray elements exist which do not have physical meanings from a topology optimization point of view. To overcome this, many approaches such as the level set method, FCM (Finite Cell Method), or BESO (Bi-Directional Evolutionary Structural Optimization) have been proposed [18]. The adaptive topology optimization method can be regarded as one of such efforts to resolve this issue [49,50]. In connection to the stress-based topology optimization, the stress distributions should be redefined with a set of adaptive elements. A recent work in [18] reported that this can causes the discontinuity in stress during optimization iterations. Next, Tsai-Wu criterion is considered for same example. Because it is difficult to determine the coefficients of the last three terms of Eq. (25), the following result can be obtained by the modified Tsai–Wu criterion using the modified coefficient, e.g., Eq. (26).

The shape of Fig. 5 using Tsai–Wu criterion is similar to that of Fig. 4 using Tsai–Hill criterion. Further, the values of the converged objective function are almost similar. Thus, it is difficult to determine the values of the coefficients used in the Tsai–Wu criterion, and there is no significant difference in the results between the Tsai–Wu and Tsai–Hill criteria. We will use the Tsai–Hill criterion in the following.

Because fiber orientation affects composite strength, it is important to consider the angle of the layers in composite design. Further, the angles of layers are included as design variables such that it changes with density simultaneously. In Fig. 4, only density is chosen as the design variable, and the angles of layers are fixed in the optimization process. In Fig. 6, however, the angles of layer change with density simultaneously. The other conditions are the same as those in Fig. 3.

Fig. 6 shows the optimization result such as the optimization shape, distribution of Tsai–Hill value, and deformed shape of an optimized

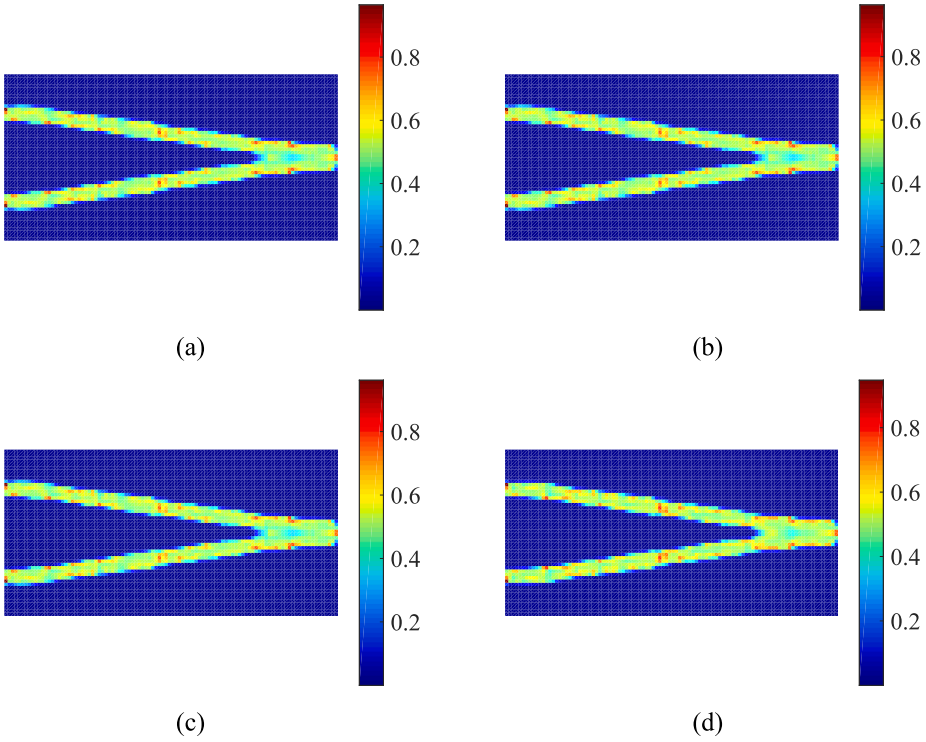

Fig. 11. Tsai–Hill value distributions for optimized layouts: (a) considering maximum Tsai–Hill value of 1st layer (maximum Tsai-Hill value: 0.9651), (b) considering maximum Tsai–Hill value of 2nd layer (maximum Tsai–Hill value: 0.9635, (c) considering maximum Tsai–Hill value of 3rd layer (maximum Tsai-Hill value: 0.9621) and (d) considering maximum Tsai–Hill value of 4th layer (maximum Tsai–Hill value: 0.9652).

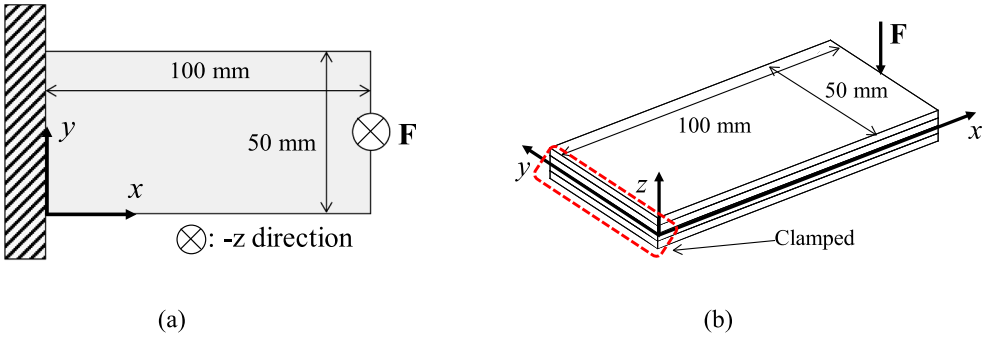

Fig. 12. Configuration of design domain and boundary conditions: (a) two-dimensional geometry of design domain and (b) three-dimensional geometry of the design domain (the number of layers is four, and the total thickness is 1 mm).

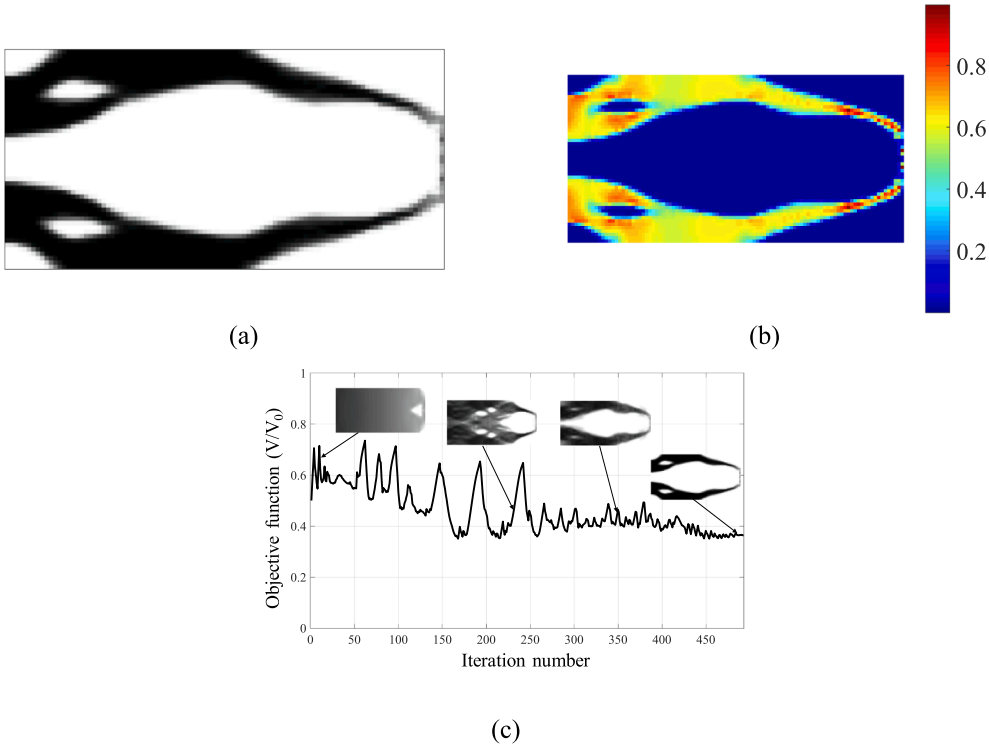

Fig. 13. Optimized shape and the Tsai–Hill value distribution considering all layers (the converged volume: 32.95% and the maximum Tsai–Hill value: 0.9956): (a) an optimized shape, (b) the distribution of Tsai–Hill value and (c) the history of the objective function.

shape when the density and angle are simultaneously changed. Compared with the result when the angles are not included as design variables, there is a slight difference in the optimized shape, and the optimized angles are [89.9977/56.8577/1.5877/89.9988]. Further, the maximum Tsai–hill value is 0.9956, which confirms that the constraint is well satisfied. However, a twisted shape of the deformed shape is confirmed in the optimized shape. Generally, it is known that a composite material can be twisted when it is laminated unsymmetrically. In the optimization result, the optimized angle is not symmetrical, and can cause twisting. Therefore, an additional symmetry condition is necessary to prevent this twisting. Applying the symmetry condition for this example yields the following result.

The optimization result is shown in Fig. 7, in which all conditions are the same as those in Fig. 6, and only the symmetry condition is additionally applied. There is a slight difference in the shape, and the maximum Tsai–Hill value is 0.9694, which shows that the constraint satisfies well. Furthermore, because the symmetry condition is included in this example, the optimized angles converge to [76.0925/18.5149/18.5149/76.0925], which satisfies the symmetry condition. In addition, owing to the symmetrical angle, the warping problem has clearly disappeared in Fig. 7(b). Therefore, a symmetric condition must be involved to avoid the warping of the unsymmetrically laminated composites. Furthermore, the local optima issue exists in topology optimization. Depending on the interpolation function, the function space of the objective and the local optima become different [40,51–53].

4.2. Example 2: Cantilever beam problem

The next numerical example considers a cantilever beam, as shown in Fig. 8 (see Fig. 8 for the detailed geometry and boundary conditions). The design domain is 100 mm × 50 mm; the left side is clamped and the load of −0.4 N acts in the y-direction at the middle of the right side. The composite laminate is 1-mm thick and consists of four layers. The angles of all layers are fixed at 0° to not consider effect of angles of layers. Furthermore, in this example, TM800s / M21 is the target material; therefore, the following values are used for the material properties of this material: E_1 = 135 GPa, E_2 = E_3 = 7.64 GPa, G_{12} =

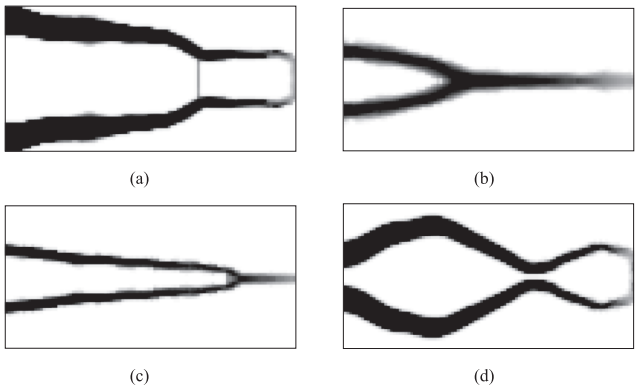

Fig. 14. Optimized shapes with different constraints: (a) considering maximum Tsai–Hill value of 1st layer (converged volume: 22.59%), (b) considering maximum Tsai–Hill value of 2nd layer (converged volume: 11.22%), (c) considering maximum Tsai–Hill value of 3rd layer (converged volume: 10.96%) and (d) considering maximum Tsai–Hill value of 4th layer (converged volume: 21.51%).

$G_{13} = 5.61$ GPa, $G_{23} = 2.75$ GPa, $\nu_{12} = \nu_{13} = 0.35$, $\nu_{23} = 0.4$, and $X = 165$ GPa, $Y = 45$ MPa, $Z = 45$ MPa, $Q = 50$ MPa, $R = 50$ MPa , $S = 50$ MPa. .

We have developed two modified p-norm approaches to calculate the representative values of these Tsai–Hill values. In this example, we apply both p-norm approaches. First, the maximum Tsai–Hill value of the whole layer is found, and when it is used as a constraint, the following optimization result can be obtained.

Fig. 9 shows that the optimized shape satisfying the constraint condition well is obtained. In contrast, using the maximum Tsai–Hill value calculated at each layer as a constraint, the following results can be obtained

The four structures in Fig. 10 show the optimum shapes when the maximum Tsai–Hill value from the first layer to the fourth layer is set as a constraint, respectively. Fig. 10 shows that all optimized results are similar in shape. This is because the distribution of the Tsai–Hill value of all layers is similar (See Fig. 11).

The distribution of the Tsai–Hill value is the same because the load applied in this example is the in-plane load. When the in-plane load is applied, the stress distribution in the thickness direction is not changed. However, when an out-of-plane load is applied, the stress changes in the thickness direction. Therefore, to observe the change in shape of each layer as described above, the out-of-plane load must be considered. In the following example, we discuss how the shape of each layer differs when an out-of-plane load is applied.

4.3. \Considering out-of-plane load

In this example, we consider a different type of load from the previous example. In the previous example, because the in-plane load was considered, the stress distributions of all layers were the same; therefore, the optimization results were the same. However, considering the out-of-plane load to be discussed in this example, the stress distribution in each layer changes. The detailed geometry and boundary conditions of this example are shown in Fig. 12. All the conditions are the same as those in Fig. 8 except that the load direction is changed from the y direction to z direction, and the magnitude is 20 N (-z direction). Further, the same material properties are used in this example. The angles of all layers are fixed at 0° not to consider effect of angles of layers (See Fig. 13).

Two modified p-norm approaches are also used in this example. As shown in the previous example, the result of using the maximum Tsai–Hill value of all layers as the constraint is as follows.

We confirmed that the optimized shape satisfying the failure constraint can be obtained. Next, the results of using the maximum Tsai–Hill value of each layer as the constraint are as follows.

From the results in Fig. 14, when the out-of-plane load is applied, the optimized shapes vary depending on which layer's maximum Tsai–Hill value is used as a constraint. The Tsai–Hill value distribution in each layer is also significantly different from that of the previous example (See Fig. 15).

With an in-plane load, there was almost no difference in the Tsai–Hill value distribution in each layer as the Tsai-Hill values and the

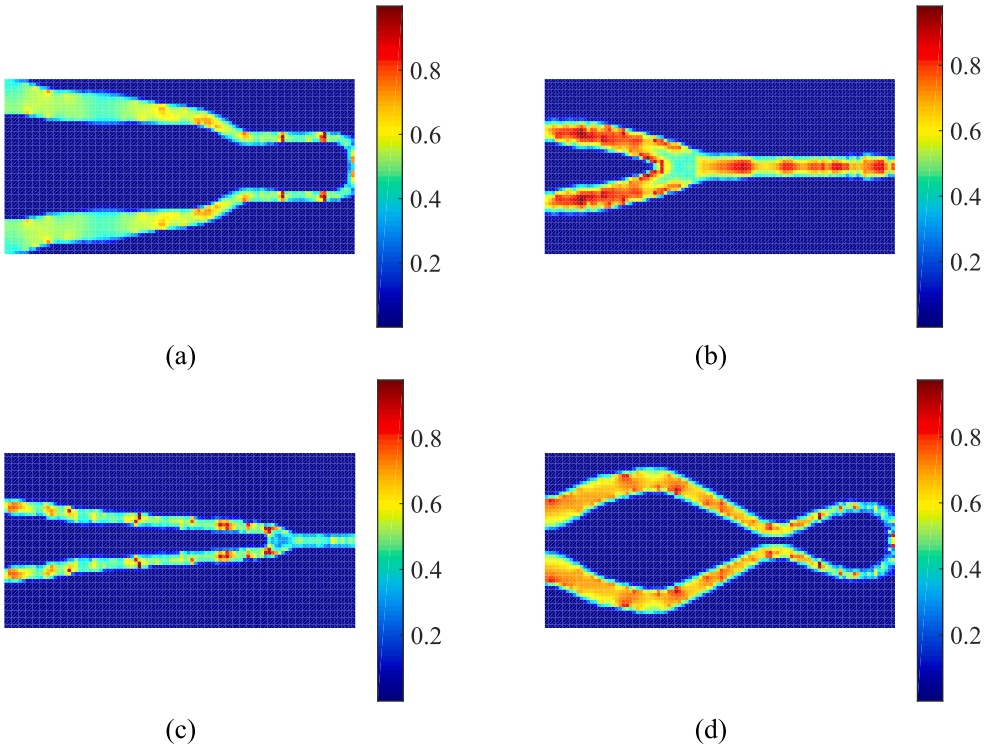

Fig. 15. Tsai–Hill value distributions for optimized layouts: (a) considering maximum Tsai–Hill value of 1st layer (maximum Tsai–Hill value: 0. 9993), (b) considering maximum Tsai–Hill value of 2nd layer (maximum Tsai–Hill value: 0. 9806, (c) considering maximum Tsai–Hill value of 3rd layer (maximum Tsai–Hill value: 0. 9759) and (d) considering maximum Tsai–Hill value of 4th layer (maximum Tsai–Hill value: 0. 9719).

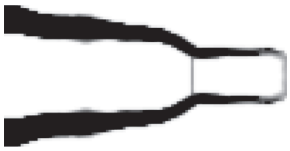

Max. Tsai-Hill value of 1st layer: 0.9993	Max. Tsai-Hill value of 2nd layer: 2.2686	Max. Tsai-Hill value of 3rd layer: 2.2686	Max. Tsai-Hill value of 4th layer: 0.9993

(a)

Max. Tsai-Hill value of 1st layer: 8.7440	Max. Tsai-Hill value of 2nd layer: 0.9806	Max. Tsai-Hill value of 3rd layer: 0.9806	Max. Tsai-Hill value of 4th layer: 8.7240

(b)

Max. Tsai-Hill value of 1st layer: 8.0724	Max. Tsai-Hill value of 2nd layer: 0.9759	Max. Tsai-Hill value of 3rd layer: 0.9759	Max. Tsai-Hill value of 4th layer: 8.0724

(c)

Max. Tsai-Hill value of 1st layer: 0.9719	Max. Tsai-Hill value of 2nd layer: 1.8152	Max. Tsai-Hill value of 3rd layer: 1.8152	Max. Tsai-Hill value of 4th layer: 0.9719

(d)

Max. Tsai-Hill value of 1st layer: 0.9349	Max. Tsai-Hill value of 2nd layer: 0.9646	Max. Tsai-Hill value of 3rd layer: 0.9646	Max. Tsai-Hill value of 4th layer: 0.9349

(e)

Fig. 16. Maximum Tsai-Hill values for all layers with result of example 2: (a) the maximum Tsai-Hill values for all layers with Fig. 14(a), (b) the maximum Tsai-Hill values for all layers with Fig. 14(b), (c) the maximum Tsai-Hill values for all layers with Fig. 14 (c), (d) the maximum Tsai-Hill values for all layers with Fig. 14(d) and (d) the the maximum Tsai-Hill values for all layers with Fig. 13(a).

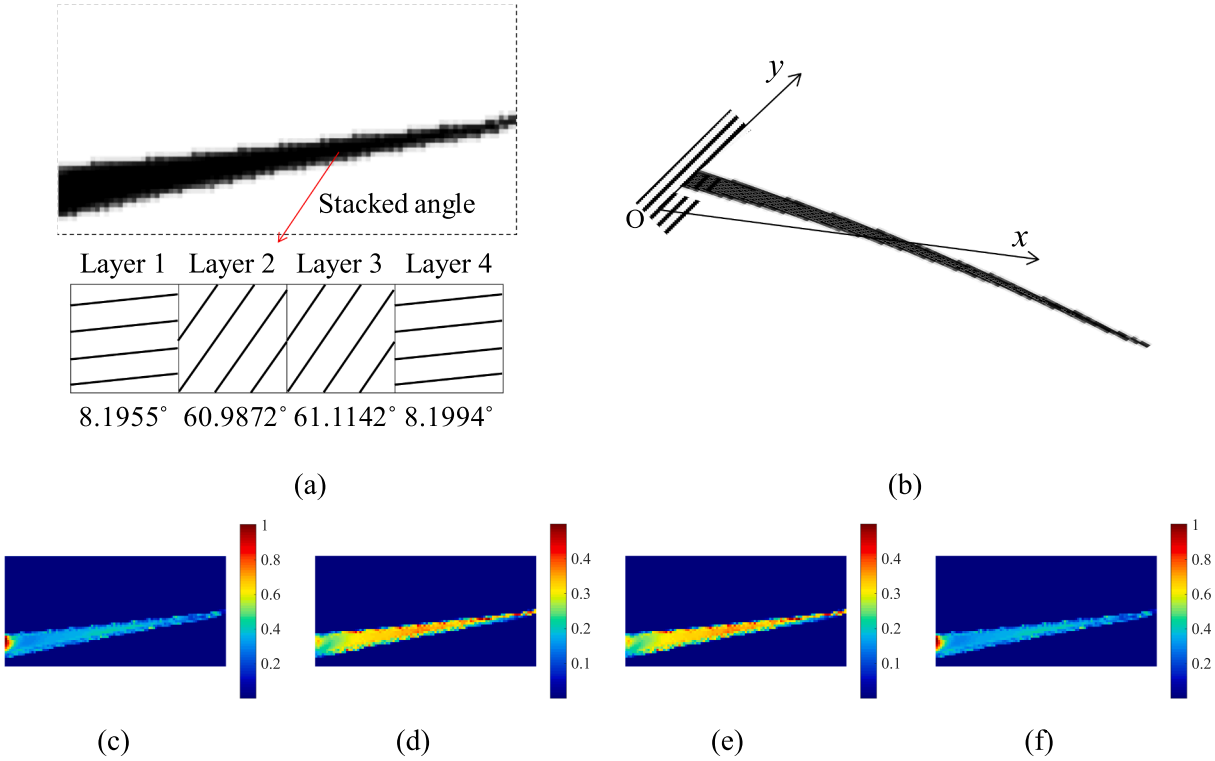

Fig. 17. An optimization result including angles as the design variable: (a) an optimized layout, (b) 3D deformation plot with the out-of-plane displacement (Deformation scaling: 1), (c, d, e, and f) the Tsai–Hill value distributions of the layer 1, 2, 3 and 4, respectively.

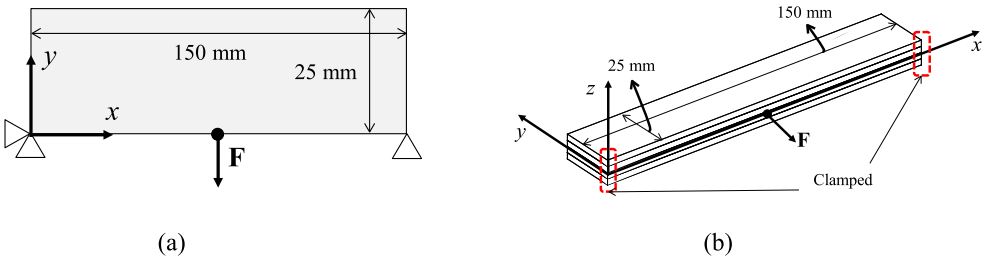

Fig. 18. Configuration of design domain and boundary conditions: (a) two-dimensional geometry of design domain and (b) three-dimensional geometry of the design domain (the number of layers is four, and the total thickness is 2.5 mm).

stress values are same along the thickness direction. With an out-of-plane load, however, the distributions of the Tsai–Hill value are different in all layers because the Tsai-Hill value and the stress values varies along the thickness direction. From this example, the different layouts are obtained due to the differences of the stress values and the Tsai-Hill values along the thickness direction. Considering the Tsai-Hill values in the first or the fourth layer, the optimized layouts use more material than the optimized layouts considering the Tsai-Hill values in the second or the third layer. Considering the stress values in the second and third layer close to the neutral plane, the optimized layout uses a less material compared with the optimized layout considering the larger stress values in the first or fourth layer. It is necessary to consider Tsai-Hill values of the other layers. Fig. 16 shows the maximum Tsai-Hill values of all layers.

Through that figure, it is known that the other layers couldn't satisfy a constraint condition even if considered layer satisfied inequality of constraint condition. In contrast, a different result can be gotten when considering all layers. From the above figure, it is necessary to find the maximum value in entire layers in order that all layers satisfy the constraint. This study develops the modified *p*-norm approach to consider some stresses of only specific layer. However, it has been confirmed that a design for preventing failure of a particular layer doesn't guarantee prevention of failures of the other layers.

To observe the effects of the angles with an out-of- plane load, the angles of all the layers are included in this example.

Fig. 17 shows the optimized layout and the optimized angles. Compared with the results with the fixed angles, a dramatic different layout can be obtained. The optimized angles are [8.1955 / 60.9872 / 61.1142 / 8.1994] and the maximum Tsai–hill values are 1.0050, 0.4998, 0.4988 and 1.0048 for the layer 1, 2, 3 and 4, respectively.

4.4. Example 3: Bridge problem

The final numerical example is a simple MBB problem, and the detailed geometry and boundary conditions are presented in Fig. 18. The design domain is 125 mm × 25 mm, and the force is 0.6 N. The

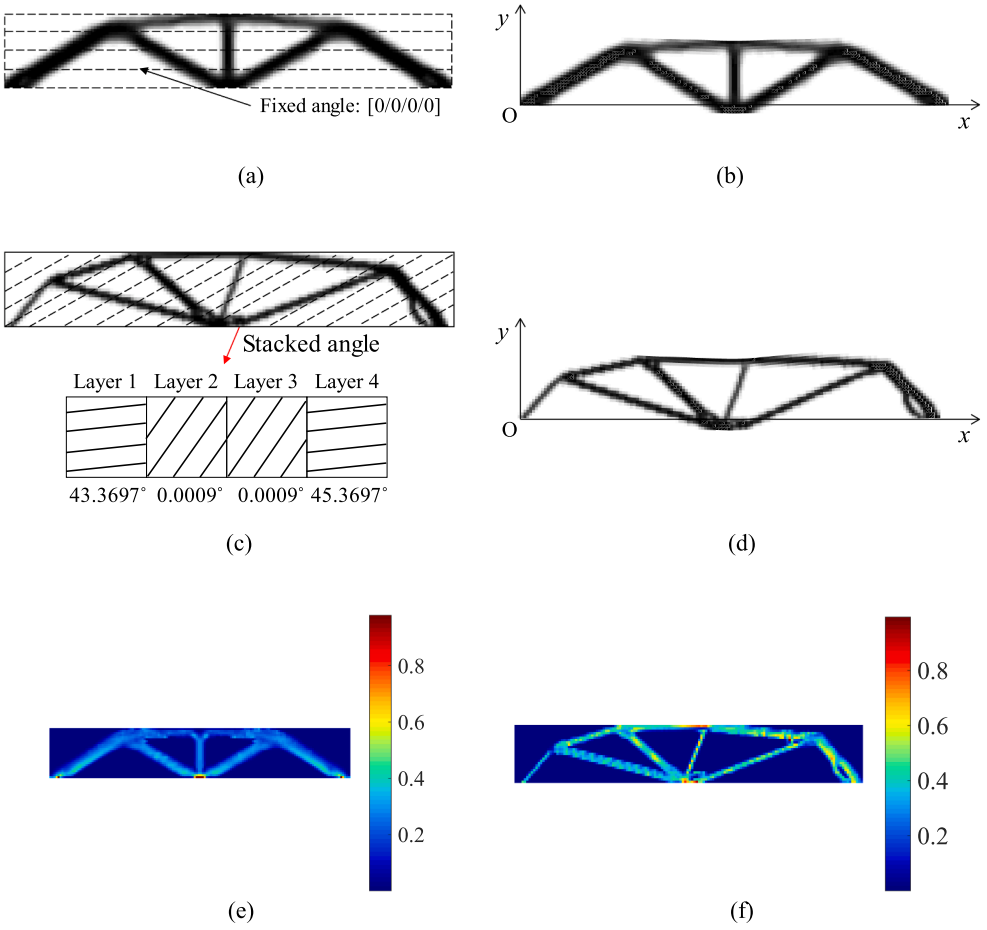

Fig. 19. Optimization results and Tsai-Hill distributions: (a) an optimization result without the angle optimization, (b) the deformed shaped of Fig. 19(a), (c) an optimization result with the angle optimization, (d) the deformed shaped of Fig. 19(c), (e) the Tsai-Hill value distribution of Fig. 19(a) and (d) the Tsai-Hill value distribution of Fig. 19(c).

thickness of the composite laminate is 2.5 mm, and this example also has four layers. In this example, the material used is TM800s / M21 as in the previous examples. Therefore, material properties used are as follows: $E_1 = 135$ GPa, $E_2 = E_3 = 7.64$ GPa, $G_{12} = G_{13} = 5.61$ GPa, $G_{23} = 2.75$ GPa, $\nu_{12} = \nu_{13} = 0.35$, $\nu_{23} = 0.4$, and $X = 165$ GPa, $Y = 45$ MPa, $Z = 45$ MPa, $Q = 50$ MPa, $R = 50$ MPa , $S = 50$ MPa. In the previous study, we confirmed that the material properties of the composite laminates are changed owing to the rotation of ply of each layer, which affects the design shape. So, in this example, we will also examine whether the rotation of each ply affects the design shape, even when considering the stress constraint problem with different design domain.

Two optimizations are performed using the example in Fig. 18. As shown in Fig. 19(a), the optimization result is obtained when the angles of all the layers are set at 0° without considering the angles in the optimization process as in the previous example. Next, optimization is performed by including the angles of each layer in the design variables. Fig. 19(b) shows the optimization result when the angle of each layer is changed during the optimization process. In this example, a symmetric condition is involved to avoid the warping of the unsymmetrically laminated composites.

Fig. 19(a) shows the optimum shape and stress distribution when the angle of all layers is set at 0°, and Fig. 19(b) shows the optimized shape and stress distribution when the angle of each layer can vary during the optimization process. In Fig. 19(a), symmetrical result is obtained because the angles of all layers are set at 0°. However, in Fig. 19(b), the angle of each layer obtained through the optimization is [45.3697/0.0009/0.0009/45.3697], and the optimized shape is asymmetrical owing to the rotation of several layers. In addition, as shown in the results of the compliance minimization problem, and confirmed in the previous research [54–56], the member in the rotated direction is thin while the member in the opposite direction is thick, as shown in Fig. 19(b). Finally, the value of the converged objective function varied depending on whether the angle of each layer is included in the optimization process. When the angle is constant, the amount of material used is approximately 31.05%, whereas when the angle is included in the optimization process; the amount of material used is approximately 21.96%, which means that the amount of material used can be reduced when the angle can be included in the optimization.

5. Conclusions

In this research, a new stress-based topology optimization method adapting the layerwise theory for composite laminates was developed. In previous studies regarding the TO method for the design of composite laminates, the classical laminate plate theory was primarily used for analysis. However, the classical laminate plate theory has been reported to exhibit limitations when applied in the analysis of composite laminates. Therefore, other theories or methods have been developed to overcome the limitations of the classical laminate plate theory. Among them, the layerwise theory, which is a newly developed theory, was applied in this study to increase the accuracy and efficiency of the analysis. An important issue in the stress-based TO method is how the maximum Tsai–Hill value can be calculated for the constraint. In

particular, in the case of composite laminates with several layers, it is necessary to choose whether to consider the stresses of all layers or the Tsai–Hill value of a specific layer; further, the maximum Tsai–Hill value used as the constraint depends on the selection. If the location of the maximum Tsai–Hill value is unknown, the maximum Tsai–Hill value must be found among all layers. In contrast, if a certain layer that has the maximum Tsai–Hill value is known, it is not necessary to consider other layers except the layer having the maximum Tsai–Hill value. In this study, we developed two types of modified *p*-norm approaches. One was developed to incorporate all layers whereas the other was created for only a particular layer. With in-plane load, theoretically all layers have the same stress distribution. Therefore, the stress value of one layer can be considered with the p-norm approach (Type 1) to compute the maximum stress value. With out-of-plane load, the stress values are different along thickness and all the stress values should be considered with the p-norm approach (Type 2). To investigate the effect of the orientations of fibers, the angles of each layer can be included as the design variable. The distinct different designs can be obtained by optimizing the angles.

Acknowledgements

This work was supported by the National Research Foundation of Korea (NRF) grant funded by the Korea government (MSIT) (No. 2018R1A5A7025522).

Appendix A. Supplementary data

Supplementary data to this article can be found online at https://doi.org/10.1016/j.compstruct.2019.111184.

References

[1] Lee DG, Suh NP. Axiomatic design and fabrication of composite structures-applications in robots, machine tools, and automobiles. Axiomatic Design and Fabrication of Composite Structures-Applications in Robots, Machine Tools, and Automobiles, by Dai Gil Lee and Nam Pyo Suh, pp 732 Foreword by Dai Gil Lee and Nam Pyo Suh Oxford University Press, Nov 2005 ISBN-10: 0195178777 ISBN-13: 9780195178777. 2005:732.
[2] Reddy JN. Mechanics of laminated composite plates. and shells: theory and analysis. CRC Press; 2004.
[3] Zhou X, Chattopadhyay A, Kim HS. An efficient layerwise shear-deformation theory and finite element implementation. J Reinf Plast Compos 2004;23:131–52.
[4] Carrera E. Evaluation of layerwise mixed theories for laminated plates analysis. AIAA J 1998;36:830–9.
[5] Kim HS, Chattopadhyay A, Ghoshal A. Characterization of delamination effect on composite laminates using a new generalized layerwise approach. Comput Struct 2003;81:1555–66.
[6] Kim HS, Chattopadhyay A, Ghoshal A. Dynamic analysis of composite laminates with multiple delamination using improved layerwise theory. AIAA journal. 2003;41:1771–9.
[7] Kim HS, Zhou X, Chattopadhyay A. Interlaminar stress analysis of shell structures with piezoelectric patch including thermal loading. AIAA J 2002;40:2517–25.
[8] Sciuva D. An improved shear-deformation theory for moderately thick multilayered anisotropic shells and plates. ASME, Trans J Appl Mech 1987;54:589–96.
[9] Xavier PB, Lee K, Chew C. An improved zig-zag model for the bending of laminated composite shells. Compos Struct 1993;26:123–38.
[10] Rupp CJ, Evgrafov A, Maute K, Dunn ML. Design of piezoelectric energy harvesting systems: a topology optimization approach based on multilayer plates and shells. J Intell Mater Syst Struct 2009;20:1923–39.
[11] Sigmund O. On the design of compliant mechanisms using topology optimization. J Struct Mech 1997;25:493–524.
[12] Takezawa A, Kitamura M. Phase field method to optimize dielectric devices for electromagnetic wave propagation. J Comput Phys 2014;257:216–40.
[13] Takezawa A, Yoon GH, Jeong SH, Kobashi M, Kitamura M. Structural topology optimization with strength and heat conduction constraints. Comput Methods Appl Mech Eng 2014;276:341–61.
[14] Wang Y, Luo Z, Kang Z, Zhang N. A multi-material level set-based topology and shape optimization method. Comput Methods Appl Mech Eng 2015;283:1570–86.
[15] Yoon GH. Maximizing the fundamental eigenfrequency of geometrically nonlinear structures by topology optimization based on element connectivity parameterization. Comput Struct 2010;88:120–33.
[16] Yoon GH, Jensen JS, Sigmund O. Topology optimization of acoustic–structure interaction problems using a mixed finite element formulation. Int J Numer Meth Eng 2007;70:1049–75.
[17] Coelho P, Guedes J, Rodrigues H. Multiscale topology optimization of bi-material laminated composite structures. Compos Struct 2015;132:495–505.
[18] Kiyono C, Vatanabe S, Silva E, Reddy J. A new multi-p-norm formulation approach for stress-based topology optimization design. Compos Struct 2016;156:10–9.
[19] Lee J, Kim D, Nomura T, Dede EM, Yoo J. Topology optimization for continuous and discrete orientation design of functionally graded fiber-reinforced composite structures. Compos Struct 2018;201:217–33.
[20] Luo Q, Tong L. A deformation mechanism based material model for topology optimization of laminated composite plates and shells. Compos Struct 2017;159:246–56.
[21] Bruggi M. On an alternative approach to stress constraints relaxation in topology optimization. Struct Multidiscip Optim 2008;36:125–41.
[22] Bruggi M, Venini P. Eigenvalue-based optimization of incompressible media using mixed finite elements with application to isolation devices. Comput Methods Appl Mech Eng 2008;197:1262–79.
[23] Bruggi M, Venini P. A mixed FEM approach to stress-constrained topology optimization. Int J Numer Meth Eng 2008;73:1693–714.
[24] Burger M, Stainko R. Phase-field relaxation of topology optimization with local stress constraints. SIAM J Control Optim 2006;45:1447–66.
[25] Cheng G, Jiang Z. Study on topology optimization with stress constraints. Eng Optim 1992;20:129–48.
[26] Duysinx P, Bendsøe MP. Topology optimization of continuum structures with local stress constraints. Int J Numer Meth Eng 1998;43:1453–78.
[27] Jeong SH, Park SH, Choi D-H, Yoon GH. Topology optimization considering static failure theories for ductile and brittle materials. Comput Struct 2012;110:116–32.
[28] Jeong SH, Yoon GH, Takezawa A, Choi D-H. Development of a novel phase-field method for local stress-based shape and topology optimization. Comput Struct 2014;132:84–98.
[29] Le C, Norato J, Bruns T, Ha C, Tortorelli D. Stress-based topology optimization for continua. Struct Multidiscip Optim 2010;41:605–20.
[30] Paris J, Navarrina F, Colominas I, Casteleiro M. Stress constraints sensitivity analysis in structural topology optimization. Comput Methods Appl Mech Eng 2010;199:2110–22.
[31] París J, Navarrina F, Colominas I, Casteleiro M. Topology optimization of continuum structures with local and global stress constraints. Struct Multidiscip Optim 2009;39:419–37.
[32] Cheng G, Guo X. ε-relaxed approach in structural topology optimization. Structural optimization. 1997;13:258–66.
[33] Duysinx P, Sigmund O. New developments in handling stress constraints in optimal material distribution. 7th AIAA/USAF/NASA/ISSMO symposium on multidisciplinary analysis and optimization1998. p. 4906.
[34] Kirsch U. On singular topologies in optimum structural design. Struct Optimization 1990;2:133–42.
[35] Rozvany G. On design-dependent constraints and singular topologies. Struct Multidiscip Optim 2001;21:164–72.
[36] Rozvany G, Sobieszczanski-Sobieski J. New optimality criteria methods: forcing uniqueness of the adjoint strains by corner-rounding at constraint intersections. Struct Optimization 1992;4:244–6.
[37] Yang R, Chen C. Stress-based topology optimization. Struct Optimization 1996;12:98–105.
[38] Li S, Atluri S. The MLPG mixed collocation method for material orientation and topology optimization of anisotropic solids and structures. Comput Model Eng Sci. 2008;30:37–56.
[39] Zheng B, Chang C-J, Gea HC. Topology optimization of energy harvesting devices using piezoelectric materials. Struct Multidiscip Optim 2009;38:17–23.
[40] Gao T, Zhang W, Duysinx P. A bi-value coding parameterization scheme for the discrete optimal orientation design of the composite laminate. Int J Numer Meth Eng 2012;91:98–114.
[41] Kiyono CY, Silva ECN, Reddy J. Design of laminated piezocomposite shell transducers with arbitrary fiber orientation using topology optimization approach. Int J Numer Meth Eng 2012;90:1452–84.
[42] Kiyono C, Silva E, Reddy J. Optimal design of laminated piezocomposite energy harvesting devices considering stress constraints. Int J Numer Meth Eng 2016;105:883–914.
[43] Kiyono C, Silva E, Reddy J. A novel fiber optimization method based on normal distribution function with continuously varying fiber path. Compos Struct 2017;160:503–15.
[44] Chattopadhyay A, Kim HS, Ghoshal A. Non-linear vibration analysis of smart composite structures with discrete delamination using a refined layerwise theory. J Sound Vib 2004;273:387–407.
[45] Huang B, Koh B-H, Kim HS. PCA-based damage classification of delaminated smart composite structures using improved layerwise theory. Comput Struct 2014;141:26–35.
[46] Shigley JE. Shigley's mechanical engineering design. Tata McGraw-Hill Education; 2011.
[47] Bhaskar K, Varadan T. A higher-order theory for bending analysis of laminated shells of revolution. Comput Struct 1991;40:815–9.
[48] Svanberg K. The method of moving asymptotes—a new method for structural optimization. Int J Numer Meth Eng 1987;24:359–73.
[49] Wang Y, Kang Z, He Q. Adaptive topology optimization with independent error control for separated displacement and density fields. Comput Struct 2014;135:50–61.
[50] Nana A, Cuillière J-C, Francois V. Towards adaptive topology optimization. Adv Eng Softw 2016;100:290–307.
[51] Wu C, Gao Y, Fang J, Lund E, Li Q. Discrete topology optimization of ply orientation for a carbon fiber reinforced plastic (CFRP) laminate vehicle door. Mater Des

2017;128:9–19.
[52] Sjølund J, Peeters D, Lund E. A new thickness parameterization for Discrete Material and Thickness Optimization. Struct Multidiscip Optim 2018;58:1885–97.
[53] Wu C, Gao Y, Fang J, Lund E, Li Q. Simultaneous discrete topology optimization of ply orientation and thickness for carbon fiber reinforced plastic (CFRP) laminated structures. ASME J Mech Des. 2018. https://doi.org/101115/14042222.
[54] Hansel W, Becker W. Layerwise adaptive topology optimization of laminate structures. Eng Comput 1999;16:841–51.
[55] Dai Y, Feng M, Zhao M. Topology optimization of laminated composite structures with design-dependent loads. Compos Struct 2017;167:251–61.
[56] Lee JW, Kim JJ, Kim HS, Yoon GH. Application of a layerwise theory for efficient topology optimization of laminate structure. J Mech Sci Technol 2019;33:711–9.